Effect of plasma treatment on electrochemical performance of lignin-based carbon fibers

Journal of Electroanalytical Chemistry 946 (2023) 117723

Contents lists available at ScienceDirect

Journal of Electroanalytical Chemistry

journal homepage: www.elsevier.com/locate/jelechem

Effect of plasma treatment on electrochemical performance of lignin-based carbon fibers

R.K. Azega [a,e,*], Mazharul Haque [a], Qi Li [c], Omid Hosseinaei [d], Hans Theliander [b,e], Peter Enoksson [a,f], Per Lundgren [a]

[a] Department of Microtechnology and Nanoscience, Chalmers University of Technology, Göteborg, Sweden
[b] Department of Chemistry and Chemical Engineering, Chalmers University of Technology, Göteborg, Sweden
[c] Smoltek Hydrogen AB, Kaserntorget 7, 411 18 Göteborg, Sweden
[d] RISE Research Institutes of Sweden, Drottning Kristinas väg 61, 114 28 Stockholm, Sweden
[e] Wallenberg Wood Science Center, Sweden
[f] Enoaviatech AB, 112 26 Stockholm, Sweden

ARTICLE INFO

Keywords:
Supercapacitor
Lignin
Carbon fiber
Wettability
Surface functional groups

ABSTRACT

The abundant and renewable nature of lignin obtained from wood renders it as a sustainable carbon resource for energy storage applications. However, their environmentally unfavorable processing conditions and limited energy storage performance prohibit the use of lignin-based carbon materials' use as supercapacitor electrodes. The material's properties require advancement to overcome the limitation of low specific capacitances. In this study, we report on the impact on the electrochemical performance of inherently hydrophobic lignin-based carbon fibers (LCF) by subjecting them to a mild plasma treatment. The electrode's capacitance was thus increased by 20%, with better rate capability and energy-power performance (11 Wh/kg and 0.8 kW/kg) in the KOH electrolyte. The quantified improvements were attributed to the capacitive functional groups, and enhanced surface wettability, which increased ion accessibility to active surface area improving charge-transfer ability to the surface with more additional functional groups. Remarkably, the selected plasma conditions introduced mostly desirable functional groups that limited any parasitic faradaic reactions prone to affect the device's long-term cycling stability and self-discharge characteristics. Furthermore, the impact of different inherent and introduced oxygen surface functional groups, including COO^{-}, C—OH, C—O, and C═O, on the capacitive performance of these fibers at different device conditions (such as cycling and electrochemical activation) was investigated in different aqueous electrolytes. To ensure environmental favorability, the electrospinning of lignin fibers was conducted using a high molecular fraction of lignin without the inclusion of any fossil-based co-spinning polymers.

1. Introduction

Carbon fibers have gained significant attention for specialized tolerances due to their exceptional tensile strength, low weight, high chemical resistance, and temperature tolerances. PAN or pitch-derived carbon fibers, known for their mechanical strength, electrical conductivity, and electrochemical characteristics, are used as electrodes in high-performing supercapacitors [1]. However, the production of carbon fibers using fossil-based precursors and unsustainable processes is environmentally unfriendly [2,3]. To address this issue, lignin, a biomass derived from renewable resources like wood, is being explored as an eco-friendly alternative. Lignin offers attractive features such as carbon-rich composition [4], redox-active functional groups [5,6], biocompatibility, thermal stability, and low toxicity [6,7]. Lignin-based fibers have been utilized in various electrochemical storage devices, including supercapacitors. However, current methods often involve the use of fossil-based additives or chemicals [8–12,43]. Electrospinning techniques can produce lignin-based carbon fibers (LCF) with advantageous properties, including high specific surface area, mechanical flexibility, and surface functional groups. The LCFs can function as both the active material and current collector, improving performance and minimizing contact resistance in supercapacitor applications [13].

* Corresponding author at: Department of Microtechnology and Nanoscience, Chalmers University of Technology, Göteborg, Sweden.
E-mail address: azega@chalmers.se (R.K. Azega).

https://doi.org/10.1016/j.jelechem.2023.117723
Received 7 June 2023; Received in revised form 8 August 2023; Accepted 15 August 2023
Available online 19 August 2023

However, their exploration in the field is currently limited [14–17]. One of the primary aims has been to enhance the electrochemical performances of LCF free from fossil-based spinning polymer to make it a more sustainable electrode choice, as aimed in this work.

Supercapacitors store energy through electrical double-layer capacitance (EDLC) and pseudocapacitance, the latter involving surface-confined redox reactions. Surface functional groups containing oxygen, such as hydroxyl, carbonyl, and quinone groups, contribute to pseudocapacitance [15]. These functional groups also enhance interfacial properties and electrode wettability. However, post high-temperature treatments besides significantly reduced tensile strength and moduli of electrospun LCF, beneficial functional groups reduce, resulting in hydrophobic electrodes that negatively affect the electrode/electrolyte interface. This behavior is especially concerning for aqueous electrolytes [18]. Therefore, optimizing surface treatment for specific electrolytes is essential to improve capacitive performance [12,19–21]. Heteroatom-doping, such as O, N, P, F, and B-doping, can reintroduce functional groups and enhance hydrophilicity and pseudocapacitive contributions [22–25]. However, common treatment methods like doping or activation can degrade or collapse the fiber morphology, impacting device performance [14,26].

Plasma treatment on the other hand is a non-invasive technique that offers significant advantages to carbon fibers in energy storage devices like supercapacitors. Numerous studies have demonstrated the modification of carbon surfaces with oxygen functional groups, which enhance electrolyte wettability and promote efficient charge transfer, thereby reducing interfacial resistance [27,28]. For instance, Ghanashyam and Jeong observed improved electrochemical performance in hydrophilic carbon fibers treated with plasma [29]. Similar studies have shown that optimized plasma treatment conditions can enhance an electrode's energy storage capacity and impedance performance by increasing the accessible active surface area, facilitating better electrolyte penetration and ion diffusion [29,30]. Another study conducted by Hsu et al. demonstrated the effectiveness of plasma treatment in introducing carboxyl and quinone functional groups, which act as redox centers and increase the specific capacitance of supercapacitors [31]. Additionally, plasma treatment is commonly used to remove contaminants, ensuring a cleaner and more uniform electrode surface. The reliability of this surface enhancement strategy for scalable industrial production is another advantage, as it requires shorter treatment durations and fewer processing steps compared to other standard methods [32]. However, it should be noted that most electrochemical studies involving plasma treatment have focused on carbon fibers derived from fossil-based polymers. Although a few investigations have explored plasma treatment of lignin-based carbon fibers, our understanding of their electrochemical performance is still limited [32,33]. Consequently, studying and comprehending the effects of oxygen plasma treatment on lignin-based carbon fibers is of great interest.

In this study, electrospun lignin-based carbon fibers were synthesized without the use of fossil-based secondary polymers. Oxygen plasma treatment offering a non-invasive and energy-efficient approach to introduce regulated oxygen functionalities to the carbon matrix, improving electrode wettability and electrode performance was tested. The surface properties of LCF were modified using low-power oxygen plasma treatment, resulting in plasma-treated lignin-based carbon fibers (PLCF). Comprehensive material characterization and electrochemical investigations were conducted, particularly using 6 M KOH as the electrolyte, to explore the positive impact of plasma treatment on capacitive performance.

2. Materials and methods

2.1. Materials synthesis

Softwood kraft lignin derived from pine/spruce mixture isolated by the LignoBoost method (Bäckhammer, Sweden) was used as the starting precursor for material synthesis. In order to extract lignin of high molecular weight, an already established sequential solvent extraction technique was carried out by dissolving 1000 g of the softwood lignin in 10 L of methanol followed by agitating for 4 h at room temperature [34]. Solids recovered from the last step after filtration was followed by treating 1 part of it with 10 times 70/30 vol methanol and methylene chloride for about 4 h. The filtered lignin from the extracted solution was concentrated using a rotary evaporator and dried in a vacuum oven for 12 h at 80 °C before proceeding to electrospinning. Detailed schematics of the extraction procedure can be found in the patent by Baker et al. [34].

2.1.1. Electrospinning and treatment of lignin fibers

A similar method as reported by Peuvot et al. was followed for the electrospinning of the polymer-free lignin fibers [35]. The extracted isolated lignin was dissolved in dimethylformamide at a concentration of 47 wt%. A cylindrical Becton Dickinson plastic syringe was filled with dissolved lignin using a KdScientific pump which fed the solution to the needle at a rate of 0.5 mL/h. The electrospun lignin fibers were collected on an aluminum foil-wrapped collector rotating at 60 rpm. A continuous electric field of 17 kV was applied between the needle and the collector which was kept 17 cm apart. The as-spun fiber mats were vacuum-dried at 105 °C for 180 min before storing them in nitrogen desiccator cabinets to avoid moisture contamination.

2.1.2. Carbonization of lignin fibers

For utilizing the lignin fibers as electrodes for supercapacitors, carbonization, and activation are essential to increase the mechanical strength, electrical conductivity, and surface area of the fibers [36]. We employ a two-step method with thermostabilization involving cross-linking reactions that extends the thermal transition points of the lignin to avoid fusing during carbonization (Fig. 1).

The dried as-electrospun lignin fiber mats were thermally stabilized in a Nabertherm Box Furnace (Labotherm L15) by heating to 250 °C with a rate of 0.5 °C/min. They were allowed to stand at that temperature for about 30 min before cooling down to room temperature. The thermostabilized lignin fibers were then transferred for carbonization to a high-temperature Thermolyne - Tube furnace. The temperature was increased from ambient to 600 °C at a rate of 3 °C/min with supplied nitrogen gas flow in the reaction tube (approximately 1.5 L/min). The fibers were allowed to stay at that temperature for 5 min to stabilize again before ramping the temperature by 5 °C/min until the carbonization temperature of 1000 °C resulting in a high BET surface area 387 m^2/g [35].The fiber mats at this point are allowed to dwell at the carbonization temperature for 20 min and are then allowed to cool down to room temperature at 20 °C/min. Afterward, the carbonized lignin fiber mats were vacuum-dried again for 3 h at 105 °C and stored in nitrogen desiccator cabinets to avoid contaminations from moisture.

2.1.3. Plasma-treatment of LCF

The post-carbonized LCF mats are hydrophobic in nature (Fig. S1 (a)). To improve the aqueous wettability of the fiber mats, oxygen plasma treatment was conducted using the Plasmatherm Batchtop RIE system. By applying a radiofrequency of 13.56 MHz and a plasma power of 25 W, the cathode was energized to generate plasma. Both sides of the fiber mat were exposed to plasma containing oxygen gas for a duration of 30 s. This treatment approach, involving a short exposure time and low power, yielded enhanced wettability (Fig. S1(b)). It was chosen deliberately to avoid the negative impact that prolonged exposures tend to cause on the mechanical and electrical properties of the fibers as observed in previous studies [37,38]. However, further optimization experiments would be necessary to fine-tune the process.

2.1.4. Supercapacitor cell assembly

Both the LCF and PLCF electrodes were used to prepare the symmetric supercapacitor devices. Electrodes with similar masses (ranging

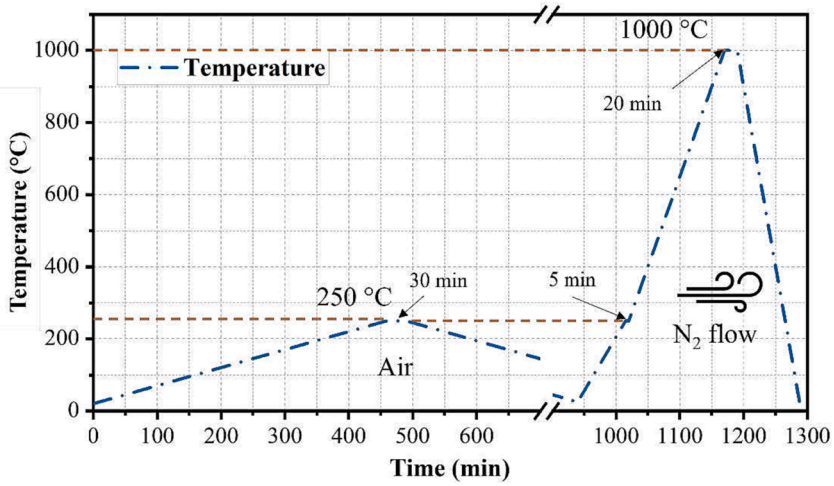

Fig. 1. LCF carbonization profile; Stabilization using Nabertherm box furnace and carbonization using Thermolyne - Open Tube/1600 °C furnace.

between 1.7 and 2.2 mg), diameters of 10 mm, and a commercially available glass fiber membrane (Whatman® GF) separator with a thickness of 200 μm and a diameter of 12 mm were used to prepare one device. To test the electrochemical performance of the prepared electrodes with different electrolytes, such as 6 M KOH, 1 M H_2SO_4, and 1 M Li_2SO_4, approximately 100 μL volumes of each electrolyte was used in different devices. The specific molarity of the KOH electrolyte was chosen to take advantage of its high ionic conductivity. The commonly reported molarities of H_2SO_4 and Li_2SO_4 were chosen to obtain an initial assessment of the electrode's compatibility in acidic and neutral electrolyte mediums. The supercapacitor devices have been assembled in CR2025 coin cells with stainless steel current collectors. All the devices were kept idle for at least 24 h before any electrochemical measurements for the complete penetration of the electrolyte into the electrodes. Electrode materials have been retrieved after all the electrochemical measurements with the help of a disassembly machine for the post-investigation of the electrode materials.

3. Characterizations

3.1. Material characterization

Surface morphology - *SEM LEO Ultra 55* was used to analyze the fiber morphology of the electrospun LCF and PLCF. The secondary electron detector was used to analyze the fiber surface in high vacuum mode while the microscope was operating at 5 kV accelerating voltage. A working distance of 6.4 mm was maintained for all samples.

The specific surface area and pore size of the fiber structures were evaluated with Brunauer-Emmett-Teller (BET) and Barrett-Joyner-Halenda (BJH) analysis using a *Micrometrics Tristar 3000*.

Functional group analysis- X-ray photoelectron spectroscopy (XPS) was used to further investigate the surface composition and chemical states of the components of interest. The PHI 5000 VersaProbe III Scanning XPS MicroprobeTM was used, which was equipped with a monochromatic AlK X-ray source with a photon energy of 1486.6 eV and a beam size of 100 μm. During the experiments, dual charge correction with an electron neutralizer and an argon ion cannon was used to compensate for the limited conductivity in non-carbonized samples. The surface composition was determined using a survey scan with a scanning energy range of 0 eV–1250 eV, a pass energy of 280 eV, and a step size of 1.0 eV. High-resolution regional scans with a pass energy of 26 eV and a step size of 0.1 eV were used to examine the chemical states of each element. The data from narrow scans were aligned with the adventitious carbon C1s peak at 284.8 eV before qualitative analysis. The system's energy scale, on the other hand, was calibrated using ISO 15472:2010, with the core levels of pure gold (Au $4f_{7/2}$), silver (Ag $3d_{5/2}$), and copper (Cu $2p_{3/2}$) set at 83.96 eV, 368.21 eV, and 932.62 eV, respectively. The MultiPakTM program was used to perform peak deconvolution. The fitted peaks were allocated to a specific energy peak location in the spectral envelope after the spectra were fitted above the Shirley background. The peak shape was fitted using a Gaussian-Lorentzian function, and the full width at half maximum (FWHM) of the peak width was less than 2.0 eV in all the fitted curves. The area ratios of the fitted peaks in the spectral envelope were used to calculate the contribution of each chemical state in a single element. The accuracy of the analyzed XPS results may result in an error bar of 0.1% to 2% due to various experimental and analytical uncertainties.

3.2. Electrochemical characterization

Electrochemical analysis- All the electrochemical measurements were conducted using a *Gamry Reference 3000AE* Galvanostat/Potentiostat workstation. Electrochemical measurements such as cyclic voltammetry (CV), and galvanostatic charge–discharge (GCD) were carried out in a wide range of scan rates (10–1000 mV/s) and current densities (0.5–5 A/g). Electrochemical impedance spectroscopy (EIS) was carried out at different states of health of the devices. The spectrum was recorded at the frequency range of 100 kHz–10 mHz at 0 V with an alternating current (ac) perturbation of 10 mV at open circuit potential. Additionally, the stability of the devices was investigated with cyclic charge–discharge (CCD) at a current density of 2 A/g for 10,000 cycles. Self-discharge characteristics of the devices were carried out by charging the devices at the rated voltage with a constant current of 0.2 A/g and immediately followed by monitoring the open circuit potential for 60 min. All the tests were carried out at room temperature (25 °C).

The specific capacitance, $C_{s,CV}$(F/g) was calculated from CV according to [39]:

$$C_{s,CV} = 4 \times 1000 \times \frac{\int_0^{2\cdot\Delta V/\nu_s} |i| dV}{2 \cdot m \cdot \Delta V} \quad (1)$$

where *I(A)* is the current response, *m* (g) is the mass of the cell's electrode, ΔV (mV) is the working voltage window, and ν (mV/s) is the scan rate.

The specific capacitance, $C_{sp,GCD}$ (F/g) from GCD curves was determined using [39]:

$$C_{s,GCD} = 4 \times \frac{I_d \cdot t_d}{m \cdot V_d} \quad (2)$$

where I_d is the discharge current, t_d is the discharge duration (s), and V_d (mV) is the discharge voltage excluding the internal resistance (IR) drop. The incorporation of the factor 4 converts the device specific capacitance to the specific capacitance attributed to a single electrode.

The power density and energy density of the devices are calculated from GCD measurements according to the following equations [39].

$$C_{device} = \frac{C_{s,GCD}}{4} \tag{3}$$

$$E = \frac{1}{2} \times \frac{C_d \bullet V_d^2}{3.6} \tag{4}$$

$$P_{avg} = 3600 \times \frac{E}{t_d} \tag{5}$$

where C_{device} is the device capacitance from the GCD measurements. E (Wh/kg) is the energy density and P_{avg} (W/kg) is the average power density of the device. The numbers 3.6 and 3600 are conversion factors for the unit of time.

4. Results and discussion

4.1. Surface morphology of PLCF

The Fig. 2 illustrates the cross-sectional view of the fibers captured using a SEM, along with the top views of LCF and PLCF, respectively. The inner and outer layers of the fibers are composed of randomly oriented fibers with approximate diameters of 1.1 μm. The plasma treatment did not visibly damage the morphology of the fibers, as there was no significant difference in appearance between LCF and PLCF fibers.

In order to investigate the compatibility of these electrodes with the aqueous solution, the contact angle measurements carried out showed a hydrophobic nature of LCF with a contact angle of 112°, while PLCF showed improved wettability with a contact angle of only 16° after a 30 s plasma treatment. Fig.S2 of the electrodes soaked in KOH electrolyte reveals that the electrolyte was well distributed along the fibers of PLCF, while in LCF, it was limited to the electrode outer layers indicating the inability of electrolyte ions to penetrate its deeper layers. The absence of visible morphological alterations in PLCF suggests that the improved compatibility with the electrolyte could be primarily due to modifications on its surface's chemical state.

4.2. Chemical characterization of oxygen plasma functionalized LCF

The quantitative surface elemental analysis was conducted using XPS. Fig. 3 presents the XPS survey spectra of both the LCF and PLCF, revealing the elemental composition of the surfaces. The narrow scan of the C1s electron orbital in Fig. 3(a) reveals a dominant signal at 285 eV, indicating the presence of sp3 hybridized C bonds. Traces of sodium were also detected in the samples, which can be attributed to residual residues from the LignoBoost processing chemicals [40]. Furthermore, additional peaks in the range of 900–1100 eV were observed in PLCF, corresponding to Na1s and O KLL peaks. These peaks suggest changes in the chemical state of the untreated LCF's chemical species after plasma treatment. The plasma treatment resulted in a notable increase in the weight percentage of oxygen in the PLCF compared to untreated LCF (Fig.S3). Importantly, this increase in oxygen content is not limited to the surface of the fiber but extends to a depth of several hundred microns within the fiber layers of the PLCF. Also, the carbon-to-oxygen (C/O) ratio of both the LCF and PLCF was relatively high compared to previous studies [33]. This discrepancy is attributed to the optimized slower heating rates for carbonization and higher plasma power conditions employed for optimal duration in this work.

The amount of oxygen in the LCF surface is significantly reduced by 70% following deoxygenation during the high-temperature carbonization. Fig. 3 (b) demonstrates that upon exposure to plasma, the C-composition in the PLCF decreases by almost 14% without any observable shift in binding energy. On the other hand, Fig. 3 (c) shows a completely different shift of the O-spectrum, where it moves in the direction of the high binding energy. The finding confirms that when fiber surfaces are treated with plasma in an oxygen atmosphere, the change in electronic environment changes the binding energy of oxygen atoms forming various oxygen containing functional groups that are known to have higher binding [37]. It should be noted that the effect of plasma treatment on the fiber surface is still highly influenced by a variety of other parameters such as power intensity and gas atmosphere which would be very interesting to investigate and requires a separate study.

The C1s and O1s spectra for LCF and PLCF are deconvoluted to identify specific functional groups and peak area ratios. As shown in Fig. 4 (a) and (b), the deconvolution of the C1s reveals numerous peaks with different binding energies.

The chemical environment of sp3 carbon (C—C) such as CH_2 groups is reflected by the peak centered at 285 eV (range between 284.6 and 285.2 eV). Furthermore, the C–OH indicating hydroxyl groups peak centers at 285.5 eV (range between 286.1 and 286.7 eV), C—O at 286.5 indicative of alcohol or ether groups, the C═O peak indicating carbonyl groups are located at 287.5 eV (range between 288.5 and 289.5 eV), and the O–C═O peak for carboxyl and esters groups is centered at 289 eV. Likewise, 531 eV (C═O), 532 eV (C—O), 533 eV (C—O—C) and 534 eV (C–OH) are the corresponding O1s peaks (Fig.S4).

Table 1 shows that the density of carboxylic acids (O═C – O) on the fiber surfaces and inner layers of PLCF experiences a slight increase of 2–4%. The prevalence of C—O and C═O groups significantly increases in PLCF, nearly both doubling. The O1s spectra further support these findings, as the atomic percentage of O—C groups increases from 3.8% in LCF to 8% in PLCF. Additionally, the atomic percent of O═C groups increases from 1.7% in LCF to 2.8% in PLCF.

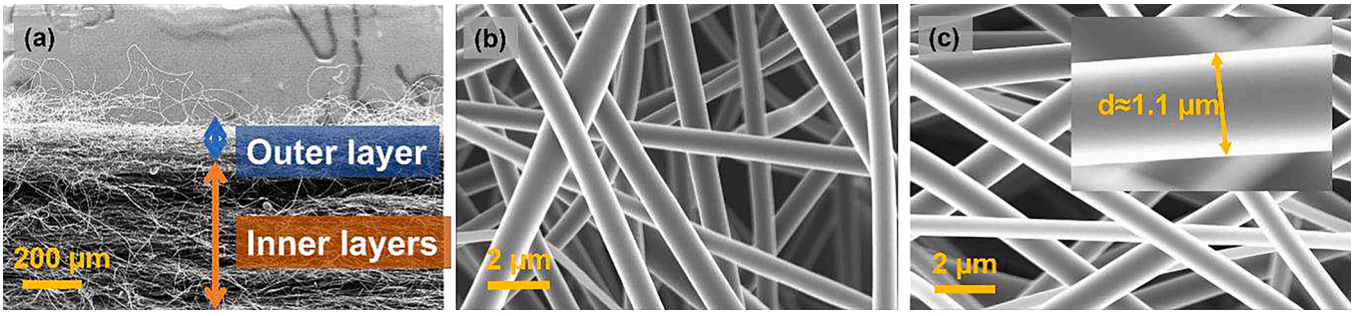

Fig. 2. SEM images (a) cross-section of electrospun LCF, (b) as-carbonized LCF, and (c) PLCF.

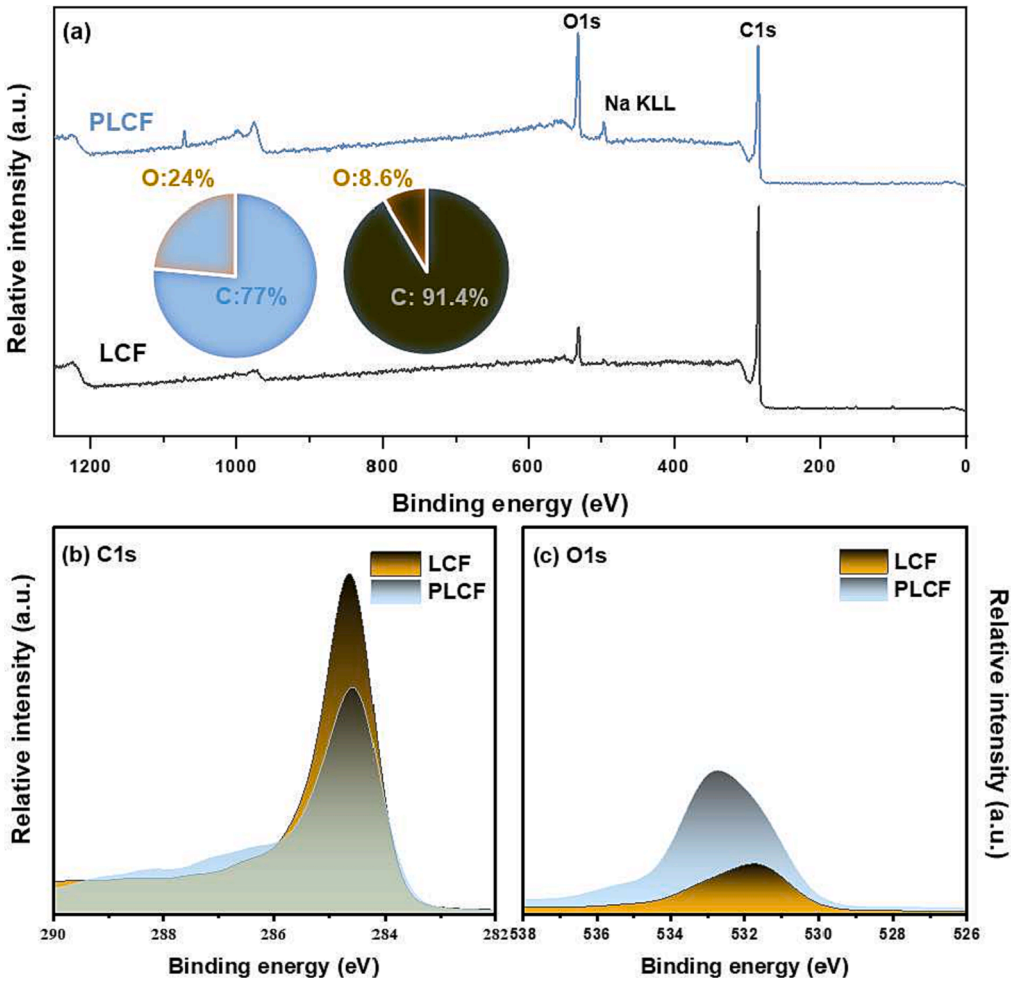

Fig. 3. XPS results showing (a) wide scan spectrum, (b) the C-spectrum, and (c) the O-spectrum of LCF and PLCF.

4.3. Electrochemical characterization of plasma functionalized LCF in KOH electrolyte

The electrochemical performance of supercapacitor cells utilizing LCF and PLCF in a 6 M KOH electrolyte was subsequently evaluated. Fig. 5(a) illustrates the CV plots of the fabricated devices, with a scan rate of 20 mV/s within the voltage range of 0–0.8 V. Both devices exhibit rectangular shapes, indicating ideal behavior consistent with EDLCs. Notably, the PLCF device displays a broader CV shape with 20% higher capacitive area, indicating enhanced capacitive properties compared to the LCF device.

In Fig. 5(b), the GCD plot depicts a linear and symmetrical charge and discharge curve for both devices at low (0.5 A/g) and high (5 A/g) currents within the rated voltage of 0.8 V. This behavior aligns with the ideal capacitive signature observed in the CV plots. Notably, the internal resistance (IR) drop is significant at high currents (LCF: 4.3 mV, PLCF: 5.2 mV) for both devices, while it is negligible at low currents (LCF: 1.2 mV, PLCF: 0.6 mV). The device utilizing PLCF electrodes exhibits a slightly higher IR drop compared to the LCF device, particularly at a high current density of 5 A/g. This discrepancy may be attributed to the presence of excess oxygen functional groups on the PLCF surface, which can contribute to an increase in the IR drop [27]. At a high current density of 5 A/g, the specific capacitance is 99 F/g for PLCF and 76 F/g for LCF. Even at the low current density of 0.5A/g, the specific capacitance remains high, with PLCF at 120 F/g and LCF at 95 F/g. These values are comparable to previous reports, indicating that the slight discrepancy in IR drop does not greatly affect the overall capacitive performance [15,33,41].

Fig. 5(c) presents the rate capability performance of the devices, indicating the capacitance retention from 10 mV/s to 1000 mV/s. The LCF device retains 60% and the PLCF device retains 68% of the capacitance. Even with increasing scan rates (as depicted in Fig.S5), PLCFs consistently demonstrate a larger capacitive area of the CV curves compared to LCF. Contrary to previous findings, where the excess of C—O and –OH surface functional groups increases the electrode's resistance [42], resulting in reduced rate performance, our results demonstrate an improved rate performance of 10% for the PLCF electrodes [28]. This validates that the higher plasma power used in our study, compared to a previous work using lower plasma power (10 W for 20 s), does not have a detrimental impact on the rate performance.

At high scan rates or currents, charge storage primarily occurs on the outer surface of the electrodes. Conversely, at low scan rates or currents, both the outer and inner layers contribute to overall charge storage as electrolyte ions have enough time to penetrate the inner layers of the electrodes. This explains the higher capacitance observed at low current densities or scan rates in the studied devices. However, operating devices at extremely low currents can result in unavoidable parasitic reactions, especially in the presence of specific surface functional groups of the aforementioned carboxyl types [33]. These parasitic reactions often lead to a high self-discharge rate, which adversely affects the overall capacitive performance. Hence, it is crucial to conduct capacitive measurements across a wide range of currents or scan rates to accurately assess the devices' performance. The capacitive properties at the lowest current provide insights into the self-discharge behavior, while the highest current indicates the rate limitation. In this context, Fig. 5(d) illustrates the self-discharge profile of both devices. After being charged

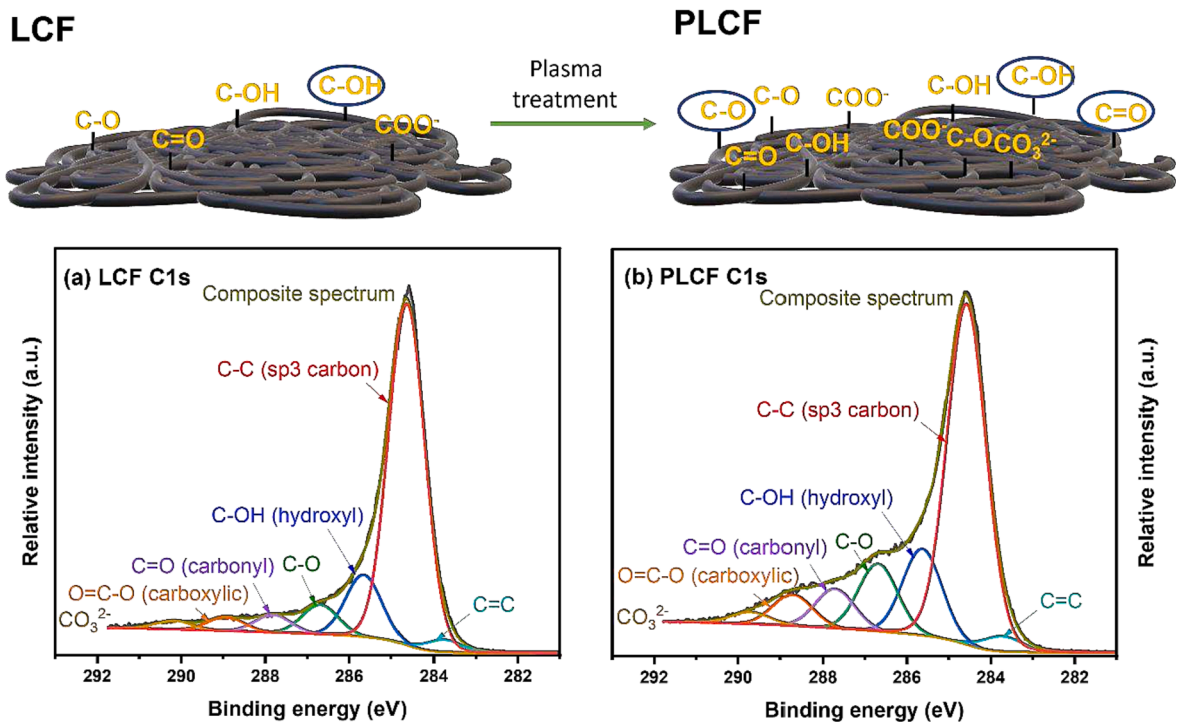

Fig. 4. The C-spectrum peaks before and after plasma treatment: (a) LCF and (b) PLCF. The experimentally acquired spectra (dashed line), peak fits for distinct chemical states of C-atoms including sp3 C (red curve), C − OH feature (blue curve), C═O feature (green curve), C═O feature (purple curve), O═C═O feature (orange curve), carbonates (yellow curve), C═C feature (fluoro-blue line), and the cumulative fit (black line). Top: Schematic representation of the predominant oxygen functional groups on the carbon fiber before and after plasma treatment. (For interpretation of the references to colour in this figure legend, the reader is referred to the web version of this article.)

Table 1
Distribution of functional groups in LCF, PLCF, and inner layers of PLCF at C1s chemical state.

Chemical state	C═C	C—C (sp^3 carbon)	C—O	C═O (carbonyl)	C—OH (hydroxyl)	O═C—O (carboxyl)	Π-Π*
LCF	2.5%	70.5%	6%	3.5%	12.5%	3%	2%
PLCF	2.5%	58%	11%	6.5%	14.5%	5%	2%
Inner layer PLCF	2%	55%	12.5%	8%	13.5%	7%	2%

to the rated voltage of 0.8 V at a constant current density of 0.2 A/g (corresponding to currents of 0.52 mA for LCF and 0.32 mA for PLCF), the devices were left in open circuit conditions without any voltage holding for 1 h. The results show that the voltage retention is 54% for LCF and 47% for PLCF. The reasonable voltage retention observed in the PLCF-containing device indicates that the introduced surface functional groups do not contribute to any parasitic reactions.

4.3.1. Surface-capacitive performance relationships

Generally, different oxygen functional groups present on the surface evolve as CO_2 or CO that directly impact the capacitive performance. CO_2 mainly originates from the carboxyl, anhydrate, and lactone groups. It has been shown that the carboxyl groups can improve the wettability of the electrodes [44]. However, its downside is it can lead to non-capacitive diffusion-controlled faradaic reactions [45]. The strongly polar double-bonded oxygen atom in carboxyl tends to lose a lone-pair electron and thus forms a positively polarized group, which then reacts with the hydroxide (OH^-) in the electrolyte solution and causes non-capacitive reactions. On the other hand, CO evolves from the phenolic hydroxyl, carbonyl, and quinone groups. Several investigations on a variety of carbon materials showed that the CO-type oxygen functional groups contribute positively to the improvement of capacitance. Also, phenolic groups aid in hydrophilicity, enhancing the surface capacitance from electrical double-layer formation without any parasitic catalytic effect [46,47]. As can be seen from Table 1 and Table S1, after plasma treatment there are lower amounts of carboxyl groups than the beneficial phenolic groups particularly the carbonyl group in the PLCF. In addition, the hydrophobic C—C bond reduces quite significantly after the plasma treatment both on the surface and in the inner layer of the PLCF [48].

Regarding charge storage, different mechanisms concurrently occur at the electrode/electrolyte interface that generally comprise of capacitive and diffusion-controlled charge storage mechanisms. In the presence of surface functional groups, the capacitive charge storage can have a contribution from both EDLC and pseudocapacitance originating from fast reversible surface-confined redox reactions. Ideally, the electrochemical signature of these charge storage mechanisms is similar, such as rectangular CV and symmetrical GCD. Depending on the types of electrodes, pseudocapacitance could also originate from the intercalation, doping in conductive polymers, and underpotential depositions, which typically involve the bulk of the electrodes and consequently display a peak in the CV and non-linearity in the GCD [49]. As this is not the case in the devices under this study, we can certainly consider that the pseudocapacitance in the capacitive charge storage could only originate from the surface-confined redox reaction of the introduced functional groups. Due to the very fast kinetics of surface-confined pseudocapacitance, it is quite complex to separate it from the EDLC. The diffusion-controlled charge storage mechanism could also originate

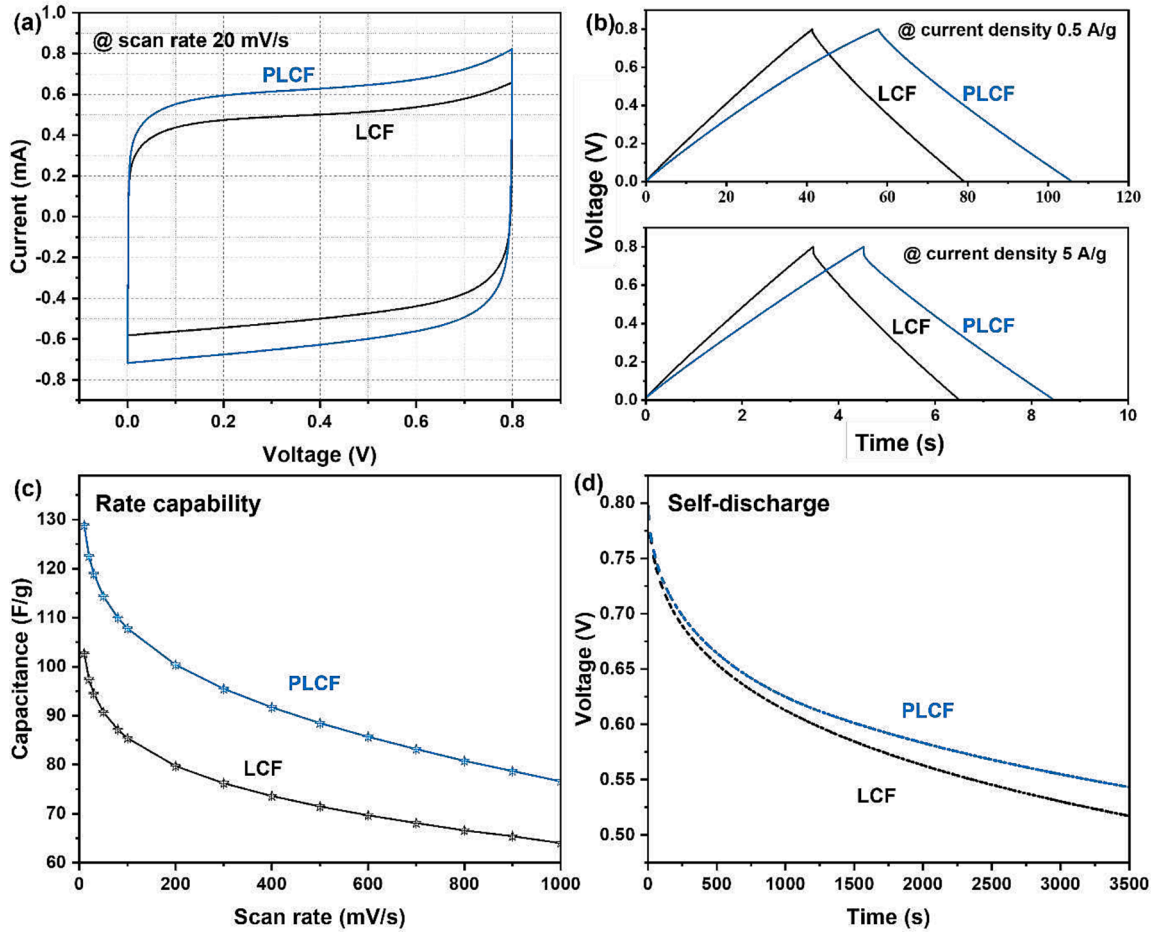

Fig. 5. Electrochemical performance of the LCF and PLCF containing devices (a) CV curves at a scan rate of 20 mV/s, (b) GCD curves at a current density of 0.5 and 5 A/g, (c) rate capability (10 to 1000 mV/s), (d) self-discharge for 1 h.

either from the bulk-redox reaction that results in a peak in the CV, or kinetic limitation at the interface. Again, as there is no visible peak in the CV of the devices under study, the diffusion limitation is most likely to originate from the kinetic limitation at the interface. Due to the different kinetics of diffusion-controlled charge storage and capacitive charge storage, it is possible to distinguish and quantify their contribution through the CV scan rate dependence on the voltammetric current according to the following equation [50]:

$$i(V) = k_1 v + k_2 v^{\frac{1}{2}} \tag{6}$$

$$i(V)/v^{\frac{1}{2}} = k_1 v^{\frac{1}{2}} + k_2 \tag{7}$$

where, *i(V)* is the current response at a specific voltage, $k_1\,\nu$, and $k_2\,\nu^{1/2}$ correspond to the current contributions from the surface capacitive effects and the diffusion-controlled process, respectively. Consequently, the capacitive and diffusion-controlled charge storage mechanisms can be obtained from the slope (k_1) and Y-intercept (k_2) of the plot of i(V)/$v^{1/2}$ versus $v^{1/2}$ at a specific voltage.

Fig. 6 demonstrates the CV curves of both the devices containing LCF and PLCF electrodes at scan rates of 10 and 500 mV/s at a voltage range of 0–0.8 V. The total current is obtained experimentally, and the capacitive currents (the shadowed regions) are determined by using equation (6). The detailed plot to extract the k_1 and k_2 values can be seen in Fig.S6.

The calculation quantitively confirms the dominance of the surface capacitive contribution. Both the LCF and PLCF-containing devices hold around 93% and 95% of capacitive current, respectively at the low scan rate of 10 mV/s, see Fig. 6 (a). These high and similar percentages of the capacitive current in both devices suggest that the observed difference in the specific capacitance between the devices should be from the extent of pseudocapacitance originating from the surface functional groups. Additionally, the capacitance improvement could also be due to the enhanced wettability of the electrodes. The impact of the wettability on the capacitive performance is more prominent at a high scan rate compared to a low scan rate as the kinetics is slow at the low scan rate which could compensate for the wettability issue to some extent. Accordingly, it can be seen from Fig. 6(b) that at the higher scan rate of 500 mV/s, the capacitive contribution increases to 96% for LCF- and 100% for the PLCF-containing device. A negligible contribution from the diffusion-limited process in the PLCF-containing device compared to the LCF-containing device suggests that the kinetic limitation is reduced with the plasma treatment to a large extent and the inner layers of the electrodes participate in the capacitive charge storage. Owing to the improved wettability and pseudocapacitive contributions of the surface functional groups, the energy performance of the device containing PLCF is shown in Fig.S7. The PLCF-containing device exhibits an energy density and power density of 11 Wh/kg and 0.8 kW/kg, while LCF exhibits 8 Wh/kg and 0.8 kW/kg at current density of 0.5 A/g. The energy and power metrics are significantly higher than the previously reported values showing 2.7 Wh/kg and 66 W/kg [28]. For a broader perspective, an analysis comparing the electrochemical performance of the PLCF supercapacitor device relative to other devices based on different blends for electrospinning lignin-based carbon fibers in the field is presented in Table S2.

At this point, it is worth mentioning the contribution of the electrolyte ions to the overall capacitive performance of the PLCF electrodes,

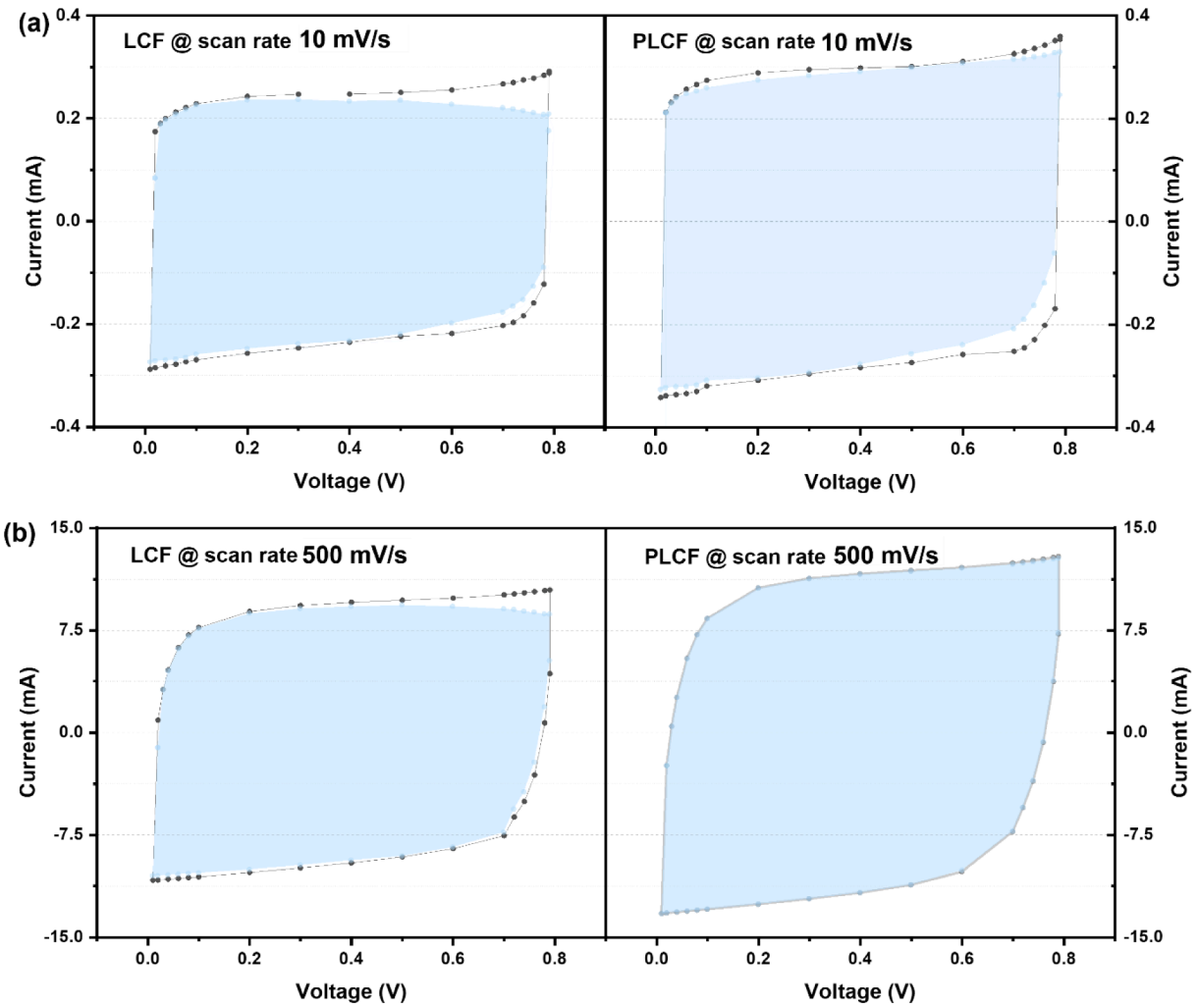

Fig. 6. Capacitive currents (regions shaded in blue) of LCF and PLCF-containing devices at scan rates of (a) 10 mV/s and (b) 500 mV/s. (For interpretation of the references to colour in this figure legend, the reader is referred to the web version of this article.)

particularly the compatibility and reactivity of certain surface functional groups with the electrolyte ions. For instance, it has been shown that mainly the carbonyl and hydroxyl groups are favorable for pseudocapacitance in a basic medium [20], such as a 6 M KOH electrolyte. The chemical reaction of these acidic functional groups, particularly –COOH (Eq. (8)) and –OH (Eq. (9)), with the alkaline electrolyte's OH^- ions can be represented as follows [51,52]:

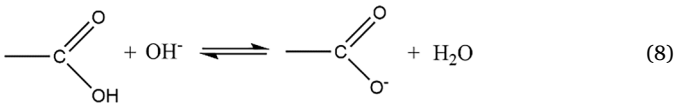

(8)

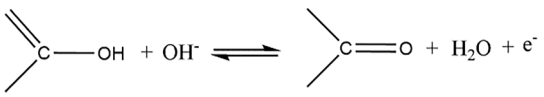

(9)

In order to verify the compatibility of the PLCF electrodes with the other types of aqueous mediums such as acidic and neutral, a brief electrochemical investigation has been carried out with 1 M H_2SO_4, and 1 M Li_2SO_4 as can be seen in Fig.S8. The capacitive properties of the acidic and neutral medium are not as impressive as the basic medium. A detailed investigation is necessary to fully understand the complex interactions at the interface with the acidic and neutral medium and therefore requires a separate study.

4.3.2. Surface-cycling performance relationship

To assess the long-term stability of the electrodes, a new set of devices was assembled using fresh electrodes. Repetitive Galvanostatic Charge-Discharge (GCD) experiments were conducted with a current density of 2 A/g, spanning a voltage range of 0–0.8 V, for a total of 10,000 cycles. Fig. 7 displays the capacitance retention and coulombic efficiency of the devices containing both electrodes. The inset in the figure depicts the GCD curve at various cycles.

The GCD curves of both devices remain linear and symmetric throughout the cycling period, indicating their structural integrity with a high coulombic efficiency of 99%. Most importantly, the capacitive performance is not degraded over the test period. This further confirms the compatibility of the electrode/electrolyte interface and validates the appropriate selection of carbonization and plasma conditions. It highlights the importance of introducing stable functional groups to prevent material degradation after cycling as observed in a previous study [33].

The LCF-containing device exhibits a stable capacitance during cycling with a marginal increase of 4%. As mentioned before, due to additional pseudocapacitance and improved wettability, the PLCF-containing device exhibits a higher capacitance of 120 F/g compared to the LCF-containing device of 95 F/g. An interesting behavior can be observed in the PLCF-containing device where the specific capacitance decreases in the initial 800 cycles and then monotonically increases up to 10% at the end of cycling. The evolution of the capacitance in this manner could be related to multiple underlying competing mechanisms

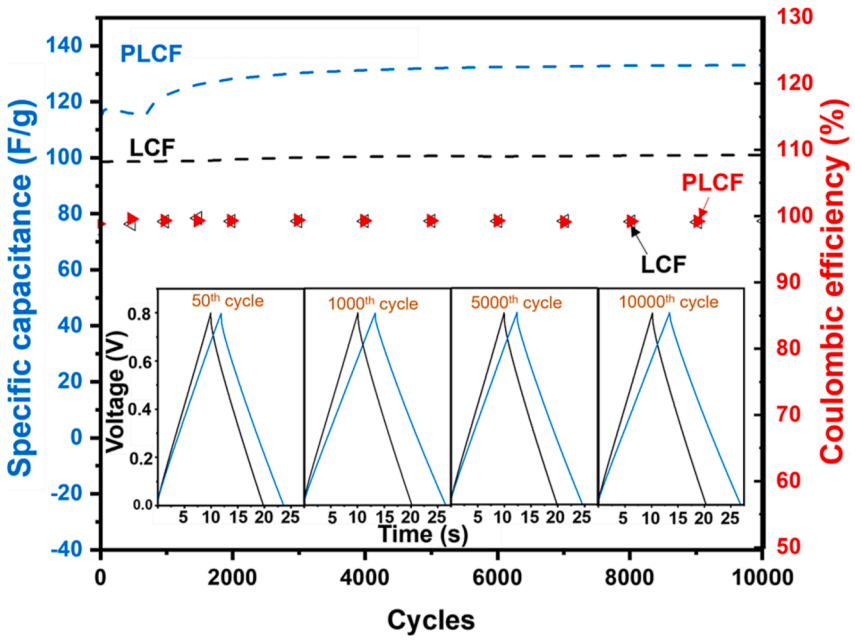

Fig. 7. Cyclic stability and coulombic efficiency of the devices containing LCF and PLCF: capacitance (left axis) and coulombic efficiency (right axis) over 10,000 cycles. Inset: charge–discharge cycles in different intervals.

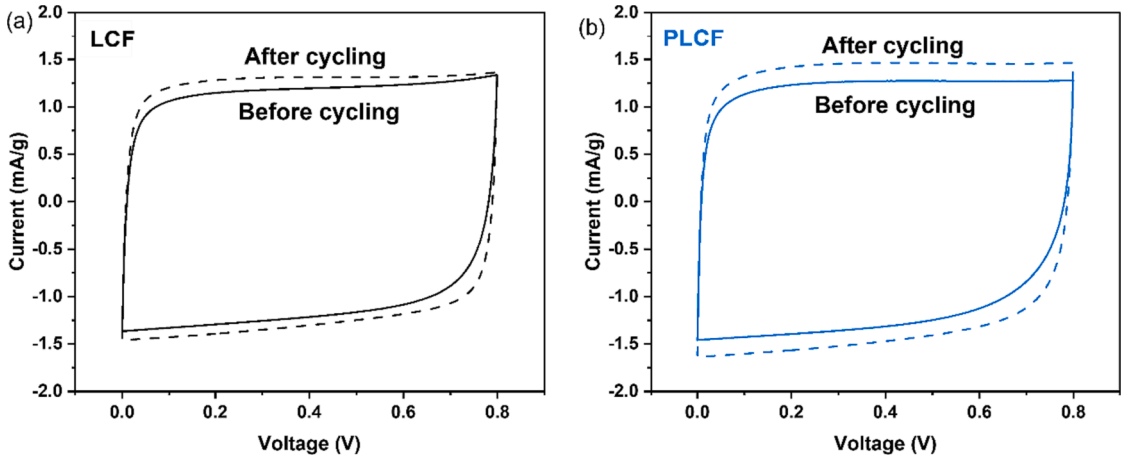

Fig. 8. CV curves comparing the capacitive current contributions of (a) LCF- and (b) PLCF- containing devices before and after undergoing 10,000 cycles.

during charge/discharge that reach equilibrium over cycling and stabilizes the capacitance. It has been shown that some of the surface functional groups such as acidic carboxyl are unstable and during the initial charge/discharge cycle they go through conversion and result in a decrease in the oxygen content [53]. Therefore, the capacitance decrease in the initial 800 cycles could be related to the reduced pseudocapacitive contribution due to the transformation and elimination of these unstable surface functional groups [54]. Afterward, the capacitance gradually increases with cycling.

In order to verify the evolution of the capacitive signature, Fig. 8 shows the CV plot of both the devices before and after 10,000 cycles with a scan rate of 10 mV/s in the voltage range of 0–0.8 V.

It can be seen that the capacitive performance of both devices has been improved as indicated by the wider CV of the devices after cycling. Consequently, the increase of the specific capacitance of the cycled PLCF-containing device is calculated to be 16%, whereas the cycled LCF-containing device is some 10% higher than the non-cycled devices. The improvement is noticed for higher scan rates as well, suggesting that the rate performance remains intact even after cycling.

The improved capacitive performance of both the devices after cycling could be related to the increased surface area that is easily accessible to the electrolyte ions as noticed in a previous study, where XPS analysis suggests that additional accumulated oxygen, CO_2, and soluble carbonates on the surface could also enhance the surface area as a result of the electrode surface etching [55]. It could also be attributed to the repeated insertions and desertions of K^+ ions in the electrode that opens up more pores as shown schematically in Fig.S9, which expands the active surface area [54] that was inaccessible for the ion penetration to the micro-sized pores (from pore size distribution data in Fig.S10) in the initial cycles. However, the extent of the capacitive improvement is larger for the PLCF-containing device. This effect is further enhanced through repetitive cycling, proposedly facilitating enhanced pore surface utilization. Furthermore, to expedite the process of maximizing pore surface utilization, electrochemical activation was implemented by subjecting a new set of devices to an elevated voltage of 1.2 V for 30 cycles at a scan rate of 20 mV/s. Following the electrochemical activation, the capacitive performance was evaluated at 0.8 V (Fig.S11) using the same scan rate. The results showed a 1.5% degradation in capacitive

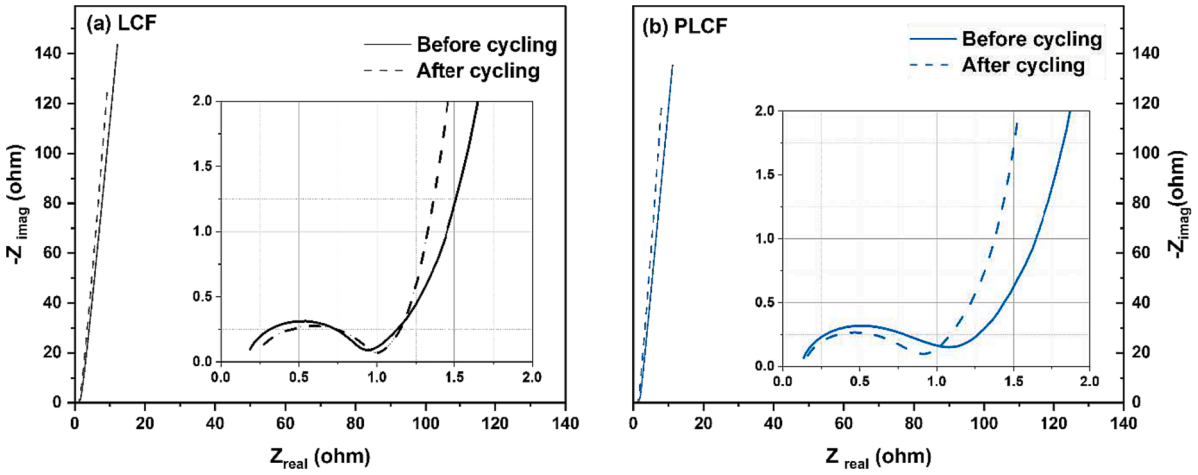

Fig. 9. Nyquist plots of (a) LCF, and (b) PLCF-containing devices before and after 10,000 cycles.

currents for LCF-containing devices while PLCF-containing devices exhibited an improvement of up to 21% compared to the capacitive currents prior to cycling at the extended voltage. Although the theoretical decomposition voltage of water is 1.23 V, in practice it can vary based on the electrodes and electrolytes involved. Therefore, the presence of surface functional groups in the PLCF may have caused the electrode potential to shift away from the electrolyte decomposition voltage during the extended voltage operation, as observed in a previous study [56].

During typical cycling tests, the device is exposed to the nominal voltage for a short duration, requiring a significant number of cycles to observe substantial effects, which can be time-consuming. However, electrochemical activation using an extended voltage can accelerate the process, although caution must be taken to avoid complete electrolyte decomposition. Nevertheless, the combination of cycling and electrochemical activation has shown a positive impact on the performance of PLCF-containing devices, resulting in improvements in both capacitive and diffusion-limited charge storage mechanisms. Further verification of this improvement can be achieved through impedance profiling of the device at different states of health.

Fig. 9 shows the Nyquist plots from the EIS measurement.

EIS provides insight into the electrolyte transport properties in the two different electrodes. In a Nyquist plot, the first intersection point in the higher frequency domain represents equivalent series resistance (ESR) that predominantly originates from the bulk electrolyte and is quite often reported as the electrolyte resistance. Commercial supercapacitors report their ESR value at 1 kHz [57]. The second intersection point of the semi-circle in the mid-frequency region is related to the interfacial resistance (R_{int}), considering the charge storage mechanism is primarily capacitive. R_{int} depends on the type of bulk electrolyte and gives a valuable understanding of the nature of the electrolyte/electrode interface. The transition from the mid-frequency region to the lowest-frequency region provides a qualitative measure of electrolyte diffusion to the electrodes.

It can be seen that the electrolyte resistance values are quite similar for both the devices before and after cycling, ranging from 0.19 to 0.27 Ω. This indicates that the electrolyte properties are not compromised during the cycling process. The ESR values extracted at 1 kHz are 0.90 Ω, and 1.0 Ω for the LCF and PLCF-containing devices respectively before cycling, while the values change to 0.95 Ω, and 0.84 Ω, after cycling. A very small increase of the R_{int} can be seen in the LCF-containing device, while a noticeable decrease of R_{int} can be seen in the PLCF-containing device, suggesting a gradual improvement of the kinetics in the interface. A significant change in the diffusion resistance can be noticed in both devices, where the diffusion resistance decreases by 2.8 Ω and 6.2 Ω in the LCF-and PLCF-containing devices after cycling. At the lowest frequency, the devices behave in a purely capacitive way where the phase angles approach 90°. Both the devices exhibit phase angle ranging from 84° to 86° before and after cycling (Fig.S12), which is nearly as ideal capacitors. The observed change of the impedance characteristics, particularly ESR, $R_{int,}$ and diffusion resistance is in agreement with the previous electrochemical measurements and reflects the positive contribution of the surface functional groups introduced by the plasma treatment.

5. Conclusion

Our study adds support for electrospun LCF as a promising electrode material for supercapacitors. To overcome the intrinsic hydrophobicity of LCF, we successfully improved its wettability by decorating the electrode surface with oxygen functional groups using a non-invasive oxygen plasma treatment. This low-power and short-duration exposure improves the capacitance of the resulting PLCF electrodes by 20% compared to LCF devices in an alkaline medium (6 M KOH) at a scan rate of 20 mV/s. The improved performance can partly be attributed to enhanced electrode kinetics, where the surface functional groups contribute to pseudocapacitive charge storage, while the contribution from inner layers of the PLCF electrodes plays a significant role for the resulting capacitive charge storage with minimal diffusion limitations. XPS analysis confirmed the presence of increased CO-type oxygen functional groups, including phenolic, hydroxyl, and carbonyl, which contributed to the capacitive performance improvement. Additionally, the lower concentration of carboxyl groups on the surface can be correlated to a slower voltage decay in the self-discharge profile. The PLCF device exhibited high cyclic stability and coulombic efficiency over 10,000 cycles, indicating that the introduced surface functional groups did not have a detrimental impact on the electrodes. Moreover, the enhanced capacitive performance after cycling validated a compatible electrode/electrolyte interface, resulting in improved pore surface utilization over repeated cycling.

While this study exemplifies the benefits of the charge storage of plasma-treated carbon fibers, there is room for further investigation into the specific plasma treatment conditions and gases employed. Additionally, a deeper understanding of the underlying mechanisms by which oxygen functional groups contribute to the enhanced capacitive performance during cycling in alkaline media would be desirable. Furthermore, future research could focus on improving the electrochemical performance of supercapacitors by incorporating pseudocapacitive metal oxides onto LCF and PLCF, which would act as a physical scaffold for composite materials. These areas present intriguing opportunities for future exploration and study.

CRediT authorship contribution statement

R.K. Azega: Conceptualization, Formal analysis, Investigation, Data curation, Validation, Writing – original draft. **Mazharul Haque:** Conceptualization, Validation, Writing – review & editing. **Qi Li:** Conceptualization, Writing – review & editing. **Omid Hosseinaei:** Methodology. **Hans Theliander:** Writing – review & editing. **Peter Enoksson:** Writing – review & editing, Funding acquisition. **Per Lundgren:** Supervision, Writing – review & editing.

Declaration of Competing Interest

The authors declare that they have no known competing financial interests or personal relationships that could have appeared to influence the work reported in this paper.

Acknowledgments

Authors acknowledge the Wallenberg Wood Science Centre's (WWSC) project 4.1.4 financially supported by the Knut and Alice Wallenberg Foundation of Sweden and the support of the European Research Council (ERC) under the European Union's Horizon 2020 Program EU Horizon 2020 project GreEnergy for this work. The authors also would like to acknowledge the technical assistance of Dr. Eric Tam for the XPS analysis. We also thank Dr. Agin Vyas for his technical support and input while carrying out this work.

Appendix A. Supplementary data

Supplementary data to this article can be found online at https://doi.org/10.1016/j.jelechem.2023.117723.

References

[1] Y. Liu, S. Kumar, Recent progress in fabrication, structure, and properties of carbon fibers, Polym. Rev. 52 (2012) 234–258, https://doi.org/10.1080/15583724.2012.705410.
[2] T. Peijs, R. Kirschbaum, P.J. Lemstra, Chapter 5: a critical review of carbon fiber and related products from an industrial perspective, Adv. Ind. Eng. Polym. Res. 5 (2) (2022) 90–106.
[3] J. Avossa, G. Herwig, C. Toncelli, F. Itel, R.M. Rossi, Electrospinning based on benign solvents: current definitions, implications and strategies, Green Chem. 24 (2022) 2347–2375, https://doi.org/10.1039/D1GC04252A.
[4] Y. Yuan, G. Zhu, Porous aromatic frameworks as a platform for multifunctional applications, ACS Cent. Sci. 5 (2019) 409–418, https://doi.org/10.1021/acscentsci.9b00047.
[5] J.P. Jyothibasu, R.-H. Wang, Y.-C. Tien, C.-C. Kuo, R.-H. Lee, Lignin-derived quinone redox moieties for bio-based supercapacitors, Polymers 14 (2022) 3106, https://doi.org/10.3390/polym14153106.
[6] H. Wang, F. Fu, M. Huang, Y. Feng, D. Han, Y. Xi, W. Xiong, D. Yang, L.i. Niu, Lignin-based materials for electrochemical energy storage devices, Nano Mater. Sci. 5 (2) (2023) 141–160.
[7] H. Liu, T. Xu, K. Liu, M. Zhang, W. Liu, H. Li, H. Du, C. Si, Lignin-based electrodes for energy storage application, Ind. Crop. Prod. 165 (2021) 113425.
[8] X. Xu, J. Zhou, L. Jiang, G. Lubineau, S.A. Payne, D. Gutschmidt, Lignin-based carbon fibers: Carbon nanotube decoration and superior thermal stability, Carbon 80 (2014) 91–102, https://doi.org/10.1016/j.carbon.2014.08.042.
[9] H. Wu, C. Liu, Z. Jiang, Z. Yang, X. Mao, L. Wei, R. Sun, Electrospun flexible lignin/polyacrylonitrile-based carbon nanofiber and its application in electrode materials for supercapacitors, Text. Res. J. 92 (2022) 456–466, https://doi.org/10.1177/00405175211037191.
[10] S. Wang, J. Bai, M.T. Innocent, Q. Wang, H. Xiang, J. Tang, M. Zhu, Lignin-based carbon fibers: formation, modification and potential applications, Green Energy Environ. 7 (2022) 578–605, https://doi.org/10.1016/j.gee.2021.04.006.
[11] C. Lai, Z. Zhou, L. Zhang, X. Wang, Q. Zhou, Y. Zhao, Y. Wang, X.-F. Wu, Z. Zhu, H. Fong, Free-standing and mechanically flexible mats consisting of electrospun carbon nanofibers made from a natural product of alkali lignin as binder-free electrodes for high-performance supercapacitors, J. Power Sources 247 (2014) 134–141, https://doi.org/10.1016/j.jpowsour.2013.08.082.
[12] S. Hu, S. Zhang, N. Pan, Y.-L. Hsieh, High energy density supercapacitors from lignin derived submicron activated carbon fibers in aqueous electrolytes, J. Power Sources 270 (2014) 106–112, https://doi.org/10.1016/j.jpowsour.2014.07.063.
[13] H. Young Jung, J. Seok Lee, H. Taek Han, J. Jung, K. Eom, Lignin-based materials for sustainable rechargeable batteries, Polymers 14 (2022), https://doi.org/10.3390/polym14040673.
[14] M. Zhu, H. Liu, Q. Cao, H. Zheng, D. Xu, H. Guo, S. Wang, Y. Li, J. Zhou, Electrospun lignin-based carbon nanofibers as supercapacitor electrodes, ACS Sustain. Chem. Eng. 8 (2020) 12831–12841, https://doi.org/10.1021/acssuschemeng.0c03062.
[15] P. Schlee, O. Hosseinaei, D. Baker, A. Landmér, P. Tomani, M. José Mostazo-López, D. Cazorla-Amorós, M.-M. Titirici, From Waste to Wealth: From Kraft Lignin to Free-standing Supercapacitors, Carbon. 145 (2019) 470–480.
[16] S. Hérou, J.J. Bailey, M. Kok, P. Schlee, R. Jervis, D.J.L. Brett, P.R. Shearing, M. C. Ribadeneyra, M. Titirici, High-density lignin-derived carbon nanofiber supercapacitors with enhanced volumetric energy density, Adv. Sci. 8 (2021) 2100016, https://doi.org/10.1002/advs.202100016.
[17] F.J. García-Mateos, R. Ruiz-Rosas, J. María Rosas, E. Morallón, D. Cazorla-Amorós, J. Rodríguez-Mirasol, T. Cordero, Activation of electrospun lignin-based carbon fibers and their performance as self-standing supercapacitor electrodes, Sep. Purif. Technol. 241 (2020), 116724, https://doi.org/10.1016/j.seppur.2020.116724.
[18] A.A. Adam, J. Ojur Dennis, Y. Al-Hadeethi, E.M. Mkawi, B. Abubakar Abdulkadir, F. Usman, Y. Mudassir Hassan, I.A. Wadi, M. Sani, State of the art and new directions on electrospun lignin/cellulose nanofibers for supercapacitor application: a systematic literature review, Polymers 12 (2020) 2884, https://doi.org/10.3390/polym12122884.
[19] R.A. Perera Jayawickramage, J.P. Ferraris, High performance supercapacitors using lignin based electrospun carbon nanofiber electrodes in ionic liquid electrolytes, Nanotechnology 30 (2019), https://doi.org/10.1088/1361-6528/aafe95.
[20] S. Ghosh, S. Barg, S.M. Jeong, K.(. Ostrikov, Heteroatom-doped and oxygen-functionalized nanocarbons for high-performance supercapacitors, Adv. Energy Mater. 10 (32) (2020) 2001239.
[21] D.-H. Kim, S. Jekal, C.-G. Kim, Y.-R. Chu, J. Noh, M.S. Kim, N. Lee, W.-J. Song, C.-M. Yoon, Facile enhancement of electrochemical performance of solid-state supercapacitor via atmospheric plasma treatment on PVA-based gel-polymer electrolyte, Gels 9 (2023) 351, https://doi.org/10.3390/gels9040351.
[22] T. Liu, K. Wang, Y. Chen, S. Zhao, Y. Han, Dominant role of wettability in improving the specific capacitance, Green Energy Environ. 4 (2019) 171–179, https://doi.org/10.1016/j.gee.2019.01.010.
[23] B. Szubzda, A. Szmaja, A. Halama, Influence of structure and wettability of supercapacitor electrodes carbon materials on their electrochemical properties in water and organic solutions, Electrochim. Acta 86 (2012) 255–259, https://doi.org/10.1016/j.electacta.2012.08.060.
[24] C.-M. Yoon, G. Lee, J. Noh, C. Lee, O.J. Cheong, J. Jang, A comparative study of the electrorheological properties of various N-doped nanomaterials using ammonia plasma treatment, Chem. Commun. 52 (2016) 4808–4811, https://doi.org/10.1039/C5CC10201D.
[25] J. Kim, G. Lee, K. Lee, H. Yu, J.W. Lee, C.-M. Yoon, S.G. Kim, S.K. Kim, J. Jang, Fluorine plasma treatment on carbon-based perovskite solar cells for rapid moisture protection layer formation and performance enhancement, Chem. Commun. 56 (2020) 535–538, https://doi.org/10.1039/C9CC07785E.
[26] Y. Li, M. Zhang, Mechanical properties of activated carbon fibers, in: Act. Carbon Fiber Text., Elsevier, 2017: pp. 167–180. https://doi.org/10.1016/B978-0-08-100660-3.00006-7.
[27] K. Okajima, K. Ohta, M. Sudoh, Capacitance behavior of activated carbon fibers with oxygen-plasma treatment, Electrochim. Acta 50 (2005) 2227–2231, https://doi.org/10.1016/j.electacta.2004.10.005.
[28] C.-C. Lai, C.-T. Lo, Plasma oxidation of electrospun carbon nanofibers as supercapacitor electrodes, RSC Adv. 5 (2015) 38868–38872, https://doi.org/10.1039/C5RA04284D.
[29] G. Ghanashyam, H.K. Jeong, Plasma treated carbon nanofiber for flexible supercapacitors, J. Energy Storage. 40 (2021), 102806, https://doi.org/10.1016/j.est.2021.102806.
[30] J. Zhou, F.u. Lu, Z. Wu, Effects of plasma on electrochemical performance of carbon cloth-based supercapacitor, Mater. Res. Express 10 (6) (2023), 065602, https://doi.org/10.1088/2053-1591/acdfbc.
[31] H.-J. Tsai, I.-H. Liao, Y.-K. Yang, D.-J. Huang, W.-K. Hsu, Comparative study on surface oxygenation and widening of carbon fibers made electrochemical electrodes, AIP Adv. 13 (2023) 035227. https://doi.org/10.1063/5.0139977.
[32] Y. Can Gorur, Surface Treatment of Softwood Lignin Based Carbon Fibers for Enhanced Interfacial Adhesion, (2017).
[33] M.W. Thielke, S. Lopez Guzman, J.P. Victoria Tafoya, E. García Tamayo, C.I. Castro Herazo, O. Hosseinaei, A.J. Sobrido, Full lignin-derived electrospun carbon materials as electrodes for supercapacitors, Front. Mater. 9 (2022), 859872, https://doi.org/10.3389/fmats.2022.859872.
[34] O. Hosseinaei, D. A. Baker, High Glass Transition Lignins and Lignin Derivatives for the Manufacture of Carbon and Graphite Fibers, n.d.
[35] K. Peuvot, O. Hosseinaei, P. Tomani, D. Zenkert, G. Lindbergh, Lignin Based Electrospun Carbon Fiber Anode for Sodium Ion Batteries, J. Electrochem. Soc. 166 (2019) A1984–A1990.
[36] F. Souto, V. Calado, N. Pereira, Lignin-based carbon fiber: a current overview, Mater. Res. Express. 5 (2018) 072001. https://doi.org/10.1088/2053-1591/aaba00.
[37] N. Dilsiz, Plasma surface modification of carbon fibers: a review, J. Adhes. Sci. Technol. 14 (2000) 975–987, https://doi.org/10.1163/156856100743013.
[38] D. Tashima, M. Hirano, S. Kitazaki, T. Eguchi, S. Kumagai, Oxygen-plasma surface treatment of an electrode sheet using carbon from japanese distilled liquor waste for double-layer capacitors, Electrochem. 1 (2020) 322–328, https://doi.org/10.3390/electrochem1030020.
[39] M. Haque, I. Abdurrokhman, A. Idström, Q.i. Li, A. Rajaras, A. Martinelli, L. Evenäs, P. Lundgren, P. Enoksson, Exploiting low-grade waste heat to produce

electricity through supercapacitor containing carbon electrodes and ionic liquid electrolytes, Electrochim. Acta 403 (2022) 139640.
[40] K.G. Latham, L. Matsakas, J. Figueira, U. Rova, P. Christakopoulos, S. Jansson, Examination of how variations in lignin properties from Kraft and organosolv extraction influence the physicochemical characteristics of hydrothermal carbon, J. Anal. Appl. Pyrol. 155 (2021), 105095, https://doi.org/10.1016/j.jaap.2021.105095.
[41] N. Thongsai, K. Hrimchum, D. Aussawasathien, Carbon fiber mat from palm-kernel-shell lignin/polyacrylonitrile as intrinsic-doping electrode in supercapacitor, Sustain. Mater. Technol. 30 (2021) e00341. https://doi.org/10.1016/j.susmat.2021.e00341.
[42] Y. Peng, Z. Chen, R. Zhang, W. Zhou, P. Gao, J. Wu, H. Liu, J. Liu, A. Hu, X. Chen, Oxygen-containing functional groups regulating the carbon/electrolyte interfacial properties toward enhanced K+ storage, Nano-Micro Lett. 13 (2021) 192, https://doi.org/10.1007/s40820-021-00722-3.
[43] P. Schlee, S. Herou, R. Jervis, P.R. Shearing, D.J.L. Brett, D. Baker, O. Hosseinaei, P. Tomani, M.M. Murshed, Y. Li, M.J. Mostazo-López, D. Cazorla-Amorós, A. B. Jorge Sobrido, M.-M. Titirici, Free-standing supercapacitors from Kraft lignin nanofibers with remarkable volumetric energy density, Chem. Sci. 10 (10) (2019) 2980–2988.
[44] R. Bagchi, M. Elshazly, J. N'Diaye, D. Yu, J.Y. Howe, K. Lian, Effects of carboxyl functionalized CNT on electrochemical behaviour of polyluminol-CNT composites, Chemistry 4 (2022) 1561–1575, https://doi.org/10.3390/chemistry4040103.
[45] L. Li, F. Li, The effect of carbonyl, carboxyl and hydroxyl groups on the capacitance of carbon nanotubes, New Carbon Mater. 26 (2011) 224–228, https://doi.org/10.1016/S1872-5805(11)60078-4.
[46] H. Oda, A. Yamashita, S. Minoura, M. Okamoto, T. Morimoto, Modification of the oxygen-containing functional group on activated carbon fiber in electrodes of an electric double-layer capacitor, J. Power Sources 158 (2006) 1510–1516, https://doi.org/10.1016/j.jpowsour.2005.10.061.
[47] S. Hoshino, K. Kawahara, N. Takeuchi, Hydrophilization of graphite using plasma above/in a solution, Jpn. J. Appl. Phys. 57 (2018) 0102B1, https://doi.org/10.7567/JJAP.57.0102B1.
[48] Q. Li, V. Kuzmenko, M. Haque, M. Di, A.D. Smith, P. Lundgren, P. Enoksson, Explanation of anomalous rate capability enhancement by manganese oxide incorporation in carbon nanofiber electrodes for electrochemical capacitors, Electrochim. Acta 340 (2020), 135921, https://doi.org/10.1016/j.electacta.2020.135921.
[49] A. Noori, M.F. El-Kady, M.S. Rahmanifar, R.B. Kaner, M.F. Mousavi, Towards establishing standard performance metrics for batteries, supercapacitors and beyond, Chem. Soc. Rev. 48 (2019) 1272–1341, https://doi.org/10.1039/C8CS00581H.
[50] T.-C. Liu, W.G. Pell, B.E. Conway, S.L. Roberson, Behavior of molybdenum nitrides as materials for electrochemical capacitors: comparison with ruthenium oxide, J. Electrochem. Soc. 145 (6) (1998) 1882–1888.
[51] C.-M. Chen, Q. Zhang, X.-C. Zhao, B. Zhang, Q.-Q. Kong, M.-G. Yang, Q.-H. Yang, M.-Z. Wang, Y.-G. Yang, R. Schlögl, D.S. Su, Hierarchically aminated graphene honeycombs for electrochemical capacitive energy storage, J. Mater. Chem. 22 (2012) 14076, https://doi.org/10.1039/c2jm31426f.
[52] Y. Fang, B. Luo, Y. Jia, X. Li, B. Wang, Q. Song, F. Kang, L. Zhi, Renewing functionalized graphene as electrodes for high-performance supercapacitors, Adv. Mater. 24 (2012) 6348–6355, https://doi.org/10.1002/adma.201202774.
[53] X. Li, Y. Jiang, P. Wang, Y. Mo, W. Lai, Z. Li, R. Yu, Y. Du, X. Zhang, Y. Chen, Effect of the oxygen functional groups of activated carbon on its electrochemical performance for supercapacitors, New Carbon Mater. 35 (2020) 232–243, https://doi.org/10.1016/S1872-5805(20)60487-5.
[54] Y. He, Y. Zhang, X. Li, Z. Lv, X. Wang, Z. Liu, X. Huang, Capacitive mechanism of oxygen functional groups on carbon surface in supercapacitors, Electrochim. Acta 282 (2018) 618–625, https://doi.org/10.1016/j.electacta.2018.06.103.
[55] B.W. Allen, C.A. Piantadosi, Electrochemical activation of electrodes for amperometric detection of nitric oxide, Nitric Oxide 8 (2003) 243–252, https://doi.org/10.1016/S1089-8603(03)00029-6.
[56] E. Raymundo-Piñero, F. Leroux, F. Béguin, A high-performance carbon for supercapacitors obtained by carbonization of a seaweed biopolymer, Adv. Mater. 18 (2006) 1877–1882, https://doi.org/10.1002/adma.200501905.
[57] A. Morandi, A. Lampasi, A. Cocchi, F. Gherdovich, U. Melaccio, P.L. Ribani, C. Rossi, F. Soavi, Characterization and model parameters of large commercial supercapacitor cells, IEEE Access 9 (2021) 20376–20390, https://doi.org/10.1109/ACCESS.2021.3053626.